Environmental Engineering and Management Journal

August 2021, Vol. 20, No. 8, 1341-1351
http://www.eemj.icpm.tuiasi.ro/; http://www.eemj.eu

"Gheorghe Asachi" Technical University of Iasi, Romania

EFFECTIVE REMOVAL OF RHODAMINE B DYE FROM AQUEOUS SOLUTION BY ADSORPTION ON α -AG_2WO_4/SBA-15 NANOMATERIAL

Francisco das Chagas Marques da Silva[1*], Lara Kelly Ribeiro da Silva[1], Anne Gabriella Dias Santos[2], Vinicius Patrício Santos Caldeira[2], Laécio Santos Cavalcante[3], Germano Pereira dos Santos[1], Geraldo Eduardo da Luz Junior[1,3]

[1]Department of Chemistry, Federal University of Piaui, 64049-550, Teresina-PI, Brazil
[2]Department of Chemistry- FANAT State University of Rio Grande do Norte, Mossoró, RN 59610-210, Brazil
[3]GERATEC-CCN-DQ, State University of Piaui, João Cabral S/N, 64002-150, Teresina-PI, Brazil

Abstract

Silver tungstate (α-Ag_2WO_4), sieve molecular mesoporous (SBA-15), and α-Ag_2WO_4/SBA-15 x% (x is mass ratio of 5, 10, and 20% of α-Ag_2WO_4 to SBA-15) were synthetized by sonochemical, hydrothermal, and post-synthesis methods, respectively. The materials were characterized by powder X-ray diffractometry (XRD), field emission electron microscopy (SEM), N_2 adsorption/desorption, X-ray photoelectron spectroscopy (XPS), and zeta potential. The characterizations verify that silver tungstate (α-Ag_2WO_4) and nanocomposite α-Ag_2WO_4/SBA-15 x% were obtained. The performance of α-Ag_2WO_4/SBA-15 x% in adsorption of RhB depended on percentage of α-Ag_2WO_4. The RhB adsorption behavior onto adsorbents was well fitted to pseudo-second order kinetics and Langmuir isotherm model. The removal efficiency of α-Ag_2WO_4/SBA-15 20% (1.050 g L^{-1}) was 100% for RhB 50 ppm at 30 min. Moreover, 80% of RhB was recuperated from adsorbents at neutral pH.

Key words: adsorbent, molecular sieve, wastewater treatment

Received: September, 2020; Revised final: February, 2021; Accepted: March, 2021; Published in final edited form: September, 2021

1. Introduction

Water pollution is global concern that causes numerous diseases. Dyes are among the major pollutants in wastewater (Rachna et al., 2018). Diverse dyes are used in textiles, leather, papermaking, plastic, food, and cosmetics industries, which are stable resisting light, heat, oxidizing agents, and generally non-biodegradable (Hayeeye et al., 2017; Zhou et al., 2019). The major source of dyes is the textile industry, which discharges large amounts of industrial wastewater (Errais et al., 2010; Shen and Gondal, 2017). The release of pollutants into public streams is a serious environmental problem, owing to the treatment for reuse and the toxicity to human and animals (Errais et al., 2010; Shen and Gondal, 2017).

Rhodamine B (RhB) is commonly used in the leather, plastic, graphics, and textile industries (Cheng et al., 2018; Silva et al., 2020a). RhB in water is an irritant to the eyes and skin and has a carcinogenic effect (Silva et al., 2020a). Other kinds of toxicity such as reproductive and neurotoxicity have been proven due to exposure to dye (Dutta et al., 2018; Silva et al., 2020b). Dyes produce an aesthetically unpleasant appearance on water, and about 1 ppm of dye tinges water (Qin et al., 2009). During dyeing operation, about 10 to 50% of the dyes are loss into wastewater, which can harm biological organisms and ecosystems. Therefore, Rhodamine B must be eliminated from water before discarding it into the environment (Cheng et al., 2018; Li et al., 2019; Qin et al., 2009).

Among the several methods to treat

* Author to whom all correspondence should be addressed: e-mail: fmarquesilva@hotmail.com; Phone: +55 86 8834-7156

wastewater, adsorption is promising due to its feasibility, flexibility, operation simplicity, cost-effectiveness, and efficiency for removing dyes and heavy metals (Silva et al., 2020a; Zhou et al., 2019). A good adsorbent has high capacity for adsorption, can quickly stabilize adsorption equilibrium, is effective for a wide range of dyes, and may easily be regenerated (Dutta et al., 2014; Zhou et al., 2019).

The literature reports the study of several adsorbents including activated carbon (Zhang et al., 2020), natural adsorbents (Periyaraman et al., 2019; Chaouki et al., 2020), zeolites (Cheng et al., 2017), magnetic $CoFe_2O_4$/grapheme oxide (GO) (Chang et al., 2020), natural and modified clay (Hamza et al., 2018), and Ag_2WO_4 (Silva et al., 2020b). Silver tungstate presents the phases: alpha (α), beta (β), and gamma (γ), among which the phase α is the thermodynamically stable (Chen and Xu, 2014; Dutta el al., 2014; Roca et al., 2015).

α-Ag_2WO_4 is versatile, and it presents several applications: antimicrobial (Foggi et al., 2017), photocatalysis (Bernard Ng and Fan, 2016), sensors (Chen and Xu, 2014), bactericide (Dutta et al., 2014), and adsorbent (Dutta et al., 2014; Silva et al., 2020b). The properties of Ag_2WO_4 in photocatalysis have been widely investigated (Andrade Neto et al., 2019; Li et al., 2016; Roca et al., 2015; Senthil et al., 2020; Xu et al., 2018; Zhu et al., 2017). The support g-C_3N_4 has been used to improve silver tungstate activity (Li et al. 2017; Zhu et al., 2017). The SBA-15 (Santa Barbara Amorphous) is an excellent support, it is type of silica with pore structure organized two-dimensional hexagonal displaying pore volume (up to 2.5 $cm^3\ g^{-1}$), external area (~1000 $m^2\ g^{-1}$), pore diameter (values of 2 until 10 nm), silica thicker wall (3 to 6 nm), and good thermal and hydrothermal stability (Silva et al., 2019; Singh et al., 2018; Zhao et al., 1998b).

Our research group (Silva et al., 2020b) has investigated the impregnation of α-Ag_2WO_4 on the SBA-15 support and its potential as an adsorbent. To date, few studies exist on the use of α-Ag_2WO_4 as an adsorbent. Dutta and coworkers reported the good adsorption capacity of α-Ag_2WO_4 to cationic dyes (Dutta et al., 2014). Silva and coworkers reported the performance of α-Ag_2WO_4/SBA-15 for adsorption of rhodamine B dye (Silva et al., 2020b); but, the influence of percentage (mass ratio) of α-Ag_2WO_4 on α-Ag_2WO_4/SBA-15 adsorption capacity has not been investigated.

Therefore, α-Ag_2WO_4 and nanocomposite α-Ag_2WO_4/SBA-15 x% (x = 5, 10, and 20) were synthesized by sonochemical and post-synthesis methods, respectively. These materials were tested to removal RhB dye from aqueous solutions to investigate the influence of percentage (mass ratio) of α-Ag_2WO_4 in the performance of α-Ag_2WO_4/SBA-15 x%. Effect of contact time, pH of the dye solution, concentration of dye, role of KCl, and temperature were also studied.

2. Experimental

2.1. Synthesis and characterizations of adsorbents

α-Ag_2WO_4 was synthetized by the sonochemical route: 0.001 mol of $Na_2WO_4.2H_2O$ and 0.002 mol of $AgNO_3$ were placed, individually, in two beakers with 100 mL deionized water. Citric acid (4.2×10^{-5} mol) already dissolved was poured to the $AgNO_3$ solution. The solutions of $AgNO_3$ and Na_2WO_4 were mixed and ultrasonicated for 3 h in a Branson (model CPX-1800H). The precipitate formed was washed several times (~15) with deionized water and dried at 65 °C for 10 h.

SBA-15 was made by hydrothermal route, in which tetraethyl orthosilicate (TEOS), Pluronic P123, HCl, and H_2O were mixed in the molar ratio 1.00:0.015:2.750:166.0. The mass of reagents was adjusted based on this molar ratio to yield 100 g of gel. The reagents P123, HCl and H_2O were mixed and magnetically stirred at 40 °C for 2 h. TEOS was placed in the mixture, which was preserved in magnetically stirred at 40 °C for 24 h. The gel yielded was poured into a Teflon flask, which was inserted in a stainless-steel autoclave and left to stand for 48 h at 100 °C. The precipitate obtained was cooled, filtered, washed with C_2H_5OH, dried at room temperature, and calcined at 500 °C for 5 h.

α-Ag_2WO_4/SBA-15 x% (x is mass ratio of 5, 10, and 20% of α-Ag_2WO_4 to SBA-15) was synthetized by post-synthesis method, in which α-Ag_2WO_4 and SBA-15 were weighed to yield 0.300 g of nanocomposite (Ag_2WO_4/SBA-15 x%) according to the aforementioned ratios. Then, the SBA-15 and α-Ag_2WO_4 were dispersed, respectively, into 50 mL and 10 mL of deionized water, and both system were ultrasonicated in an equipment Branson (model CPX-1800H) for 30 min. After that, the dispersion of α-Ag_2WO_4 was poured in dispersion of SBA-15, and the resulting suspension was magnetically stirred at 80 °C until the water evaporated, and obtained powder was dried at 100°C for 6 h.

The adsorbents were characterized by powder X-ray diffractometry (XRD), N_2 adsorption-desorption, field emission Scanning electron microscopy (SEM), X-ray photoelectron spectroscopy (XPS), and zeta potential. X-ray diffraction were collected by Rigaku diffractometer with Cu-Kα radiation, 30 mA and 40 kV. Scanning electron microscopy (SEM) was executed with instrument FE-SEM, FEI, Quanta FEG 250. N_2 adsorption-desorption at 77 K was performed in an equipment ASAP2010 from Micromeritics. The specific surface area and distribution of the pore size were obtained, respectively, by BET (Brunauer, Emmett and Teller) and BJH (Barrett, Joyner and Halenda) methods. XPS analysis is based in photoelectric effect, which allowed to know the state of elements on surface of materials synthetized, well as to investigate

interactions between components in composites. X-ray photoelectron spectroscopy (XPS) data were obtained in instrument Thermo Fischer Scientific, model K-alpha, using monochromatic radiation of Mg-Kα (1253.6 eV). Zeta potential was performed with the equipment Horiba Nanoparticle analyzer SZ-100, before of analysis, 2 mg of adsorbent was inserted in plastic tube (Falcon) with 50 mL of deionized water (pH ~ 6), which was ultrasonicated in an equipment Branson ultrasonic (model CPX-1800H) for 30 min with a frequency of 42 Hz.

2.2. Adsorption experiments

The adsorption tests were conducted by a mixture of 7 mg of α-Ag_2WO_4, α-Ag_2WO_4/SBA-15 x% (x = 5, 10, and 20), SBA-15, and 50 mL of aqueous solutions of the RhB dye, analogous to research of Dutta and coworkers (2014). The blend was stirred (200 rpm at 25 ± 1°C), in the dark, until equilibrium was attained. The RhB concentration was measured in an UV-vis spectrophotometer. The tests were performed in triplicate, and adsorption capacity (q_e mg g^{-1}) was determined using Eq. (1):

$$q_e = \frac{(C_0 - C_e)V}{m} \quad (1)$$

where, V is volume (L), C_0 and C_e are, respectively, initial and equilibrium dye concentrations (mg L^{-1}), and m (g) is mass of adsorbent.

The removal efficiency (*Re%*) was defined by Eq. (2):

$$Re(\%) = \frac{(C_0 - C_e)}{C_0} \times 100 \quad (2)$$

The study about the effect of contact time used dye concentrations 2.5, 5, 10, 15, and 20 mg L^{-1}, similar to the work of Sousa et al. (2018), pH = 3.5, in 5, 10, 20, 40, and 60 min. To test the effect of pH (to α-Ag_2WO_4 and α-Ag_2WO_4/SBA-15 20%), we fixed the RhB concentration at 20 mg L^{-1} adjusted and the pH of the RhB solution (pH = 1, 3, 3.5, 5, 7, and 9) by adding HCl or NaOH (0.5 mol L^{-1}). Study kinetics fixed RhB concentration at 20 mg L^{-1}, pH = 3.5, and time (2, 4, 6, 8, and 10 min.) for α-Ag_2WO_4 (5, 10, 15, 30, and 60 min.), for α-Ag_2WO_4/SBA-15 x% (x = 5, 10, and 20), and SBA-15. Pseudo-first order and pseudo-second order models were investigated, which are described by Eqs. (3) and (4) (Ho and Mckay, 1998; Sousa et al., 2018):

$$ln(q_e - q_t) = ln\, q_e - K_t t \quad (3)$$

$$\frac{t}{q_t} = \frac{1}{k_2 q_e^2} + \frac{t}{q_t} \quad (4)$$

where: q_e (mg g^{-1}) is adsorption capacity at equilibrium; q_t (mg g^{-1}) is adsorption capacity in time t; K_1 and K_2 are kinetics constants, respectively, of first-order and second-order.

To investigate the isotherm type, time was fixed at 15 min, pH = 3.5, and dye concentrations 2.5, 5, 10, 15, 20, 30, 40, and 50 mg L^{-1} for α-Ag_2WO_4; SBA-15 and α-Ag_2WO_4/SBA-15 x% (x = 5, 10, and 20), aqueous solutions of RhB (2.5, 5, 10, 15, and 20 mg L^{-1}) at 60 min. The models Langmuir (Eq. 5), Freundlich (Eq. 6), and Temkin (Eq. 7) isotherms were evaluated for adsorption data (Cheng et al., 2018; Freundlich, 1926; Langmuir, 1916; Sousa et al., 2018):

$$\frac{C_e}{q_e} = \frac{C_e}{q_m} + \frac{1}{q_m K_L} \quad (5)$$

$$log\, q_e = \frac{1}{n} log\, C_e + log\, K_f \quad (6)$$

$$q_e = B\, ln\, K_T + B\, ln\, C_e \quad (7)$$

where q_m (mg g^{-1}) and K_L (L mg^{-1}) are, respectively, Langmuir constants related to the maximum adsorption capacity and energy of adsorption; K_f and n are the Freundlich constants representing, respectively, the adsorption capacity (L g^{-1}) and adsorption intensity; K_T (L g^{-1}), R (8.314 J mol^{-1} K^{-1}), and T (K) are, respectively, Temkin constants related to equilibrium binding constant, gas constant, and absolute temperature, and b is heat of adsorption, B = RT/b (Hayeeye et al., 2017; Peng et al., 2016; Shen and Gondal, 2017; Sousa et al., 2018).

The dimensionless separation factor (R_L) indicates the favorability of adsorption (Eq. 8) (Hayeeye et al., 2017).

$$R_L = \frac{1}{1 + KC_0} \quad (8)$$

The study about effect of temperature used the following specification fixed pH = 3.5; temperatures of 298, 308, and 318 K; and dye concentration of 40 mg L^{-1} (α-Ag_2WO_4/SBA-15 20% and α-Ag_2WO_4) and 20 mg L^{-1} (SBA-15). The Gibbs free energy (ΔG), enthalpy (ΔH), and entropy (ΔS) were calculated by Eqs. (9-11):

$$\Delta G = - RT\, ln\, K \quad (9)$$

$$K = \frac{q_e}{C_e} \quad (10)$$

$$\Delta G = \Delta H - T\Delta S \quad (11)$$

where K is the equilibrium constant. The parameter ΔH and ΔS were determined through of graph ($ln\, K$ versus T^{-1}), which the linear and angular coefficient are, respectively, ΔS/R and ΔH/R (Hayeeye et al., 2017; Inyinbor et al., 2015; Sousa et al., 2018).

In dosage tests, α-Ag_2WO_4 or α-Ag_2WO_4/SBA-15 20% (0.140, 0.176, 0.352, 0.700, and 1.050 g L^{-1}) were mixed with 50 mL of RhB 50 mg L^{-1}, pH 3.5, for 30 min. To investigate the role of KCl in adsorption, RhB and KCl solutions were mixed to ensure 50 mL of solution with RhB concentration equal to 40 mg L^{-1} (α-Ag_2WO_4/SBA-15 20% and α-Ag_2WO_4) and concentrations of KCl (0; 0.2; 0.4, and 0.8 mol L^{-1}); the time of each test was 30 min. Desorption tests were performed by changing the pH. The pH of the solution, after the end of adsorption experiment, was adjusted (to 7, 10, and 12, with NaOH 0.5 molL^{-1}), promoting instantly desorption of RhB from adsorbents. The dye concentration was determined by UV-vis analysis.

3. Results and discussion

3.1. Powder X-ray diffractometry (XRD)

Diffractograms at small and wide angle XRD patterns of adsorbents are presented in Fig. 1.

The three XRD peaks referring to (100), (110), and (200) planes are assigned to the hexagonal arrangement mesoporous and pore of structures peculiar to SBA-15 (Silva et al., 2020b; Zhao et al., 1998a). The diffractogram of α-Ag_2WO_4/SBA-15 x% (x = 5, 10, and 20) like pure SBA-15 matrix reveals conservation of the mesoporous structure of SBA-15 (Jin et al., 2019). The diffractogram of silver tungstate, Fig. 1b, agrees well with α-Ag_2WO_4 crystals without any deleterious phase, orthorhombic structure, space group (*Pn*2*n*), and the point group symmetry (C_{2v}) (Inorganic Crystal Structure Database - ICSD card Nº. 4165) (Macedo et al., 2018; Skarstad and Geller, 1975). SBA-15 presents a broad XRD peak, at 2θ ≈ 22.6º, characteristic of amorphous silica (SiO_2). α-Ag_2WO_4/SBA-15 x% presents peaks relative to SBA-15 and α-Ag_2WO_4. The diffractograms verify that of SBA-15, α-Ag_2WO_4 and α-Ag_2WO_4/SBA-15 x% were obtained.

3.2. Scanning electron microscopy (SEM)

The micrographs of SEM are presented in Fig. 2. α-Ag_2WO_4 nanocrystals usually present morphology of rods (Foggi et al., 2017; He et al., 2016; Longo et al., 2014), but Fig. 2a shows several agglomerated nanocrystals without defined format, which must be related to the use of citric acid in the formation of α-Ag_2WO_4. Fig. 2b displays the characteristic structure of SBA-15, which is skeletal formats and unidirectional cylindrical channels (Costa et al., 2018; Silva et al., 2020b). Figs. 2(c-e) illustrates that α-Ag_2WO_4/SBA-15 x% maintained the arrangement of SBA-15 with the external surface impregnated of α-Ag_2WO_4 nanocrystals. This result is in harmony with XRD.

3.3. N_2 adsorption-desorption

Table 1 presents the properties textural and zeta potential of adsorbents. Table 1 shows that α-Ag_2WO_4 has a surface area of 21.0 m^2 g^{-1}, similar to the surface area of Ag_3PO_4 (Chai et al., 2015). α-Ag_2WO_4/SBA-15 x% (x = 5, 10 and 20) presents textural properties (micropore volume (V_{micro} cm^3 g^{-1}), pore volume (V_{pore} cm^3 g^{-1}), micropore area (S_{micro} m^2 g^{-1}), and surface area (S_{BET} m^2 g^{-1})) smaller than SBA-15. This indicates that α-Ag_2WO_4 promotes the blockage of pores in the SBA-15, because it was mostly impregnated on the external area of support (SBA-15) (Araújo et al., 2016; Costa et al., 2018; Silva et al., 2020b). This is corroborated by SEM analysis (Fig. 2(c-e)).

All zeta potentials (Table 1) are negative. Thus, in solution, the adsorbents have a negatively charged surface. The dissolution of α-Ag_2WO_4 in WO_4^{2-} and Ag^+ generates the negative potential of silver tungstate (Dutta et al., 2014; Silva et al., 2020b; Xu et al., 2015). The negative potential of SBA-15 is attributed to the groups of deprotonated silanols and OH^- bonded on the external surface of the support (Szewczyk et al., 2019).

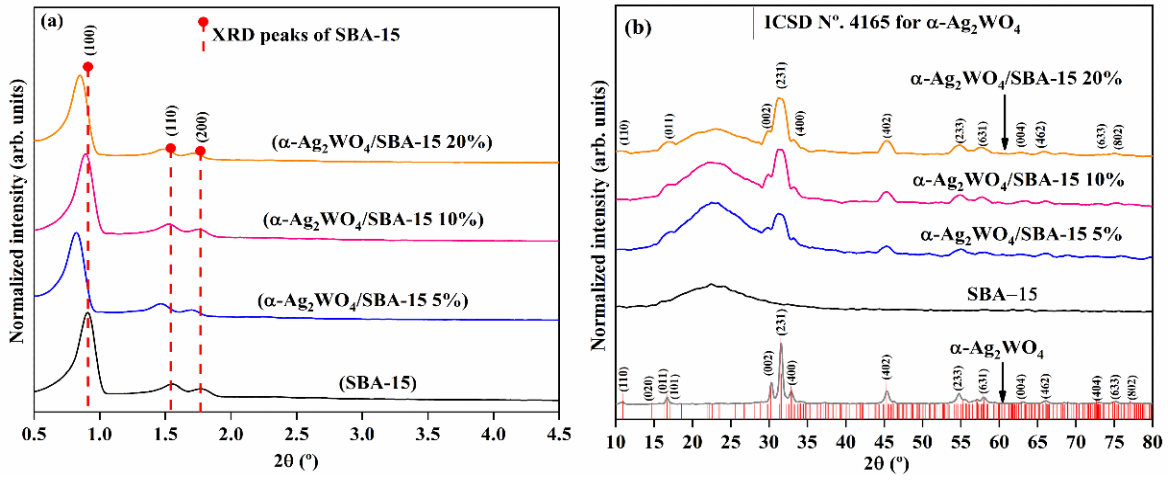

Fig. 1. Small (a) and wide (b) angle XRD patterns of adsorbents

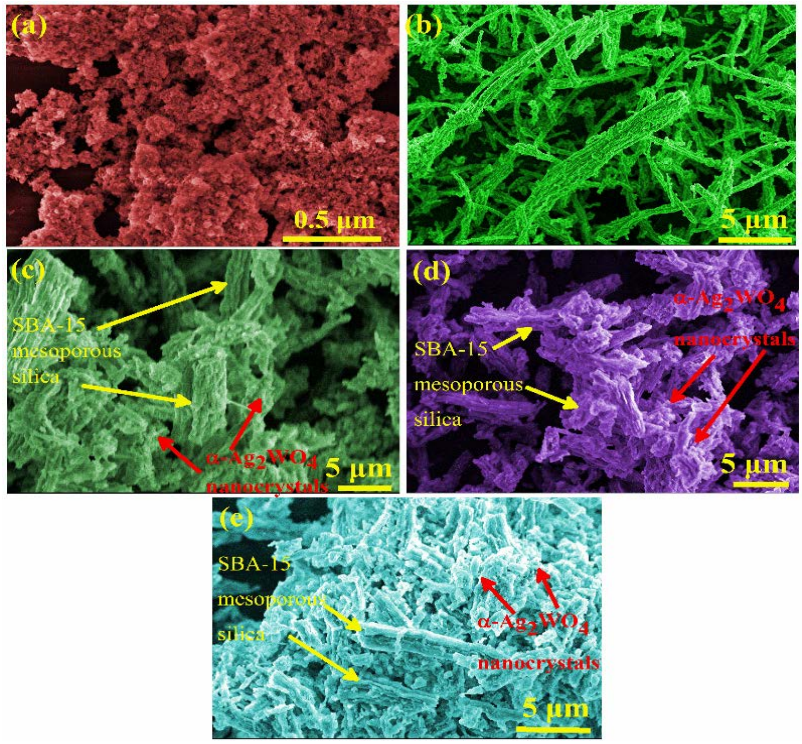

Fig. 2. SEM for (a) α-Ag_2WO_4, (b) SBA-15, (c) α-Ag_2WO_4/SBA-15 5%, (d) α-Ag_2WO_4/SBA-15 10%, and (e) α-Ag_2WO_4/SBA-15 20%

3.4. X-ray photoelectron spectroscopy (XPS)

The signal characteristics of Ag, W, O, and Si in the spectra illustrated in Fig. 3 demonstrate the coexistence of α-Ag_2WO_4 and α-Ag_2WO_4/SBA-15 x%. The carbon present in all samples may be derived from the carbon containing compounds used as the internal standard (Xu et al., 2018). α-Ag_2WO_4/SBA-15 x% exhibit signals present in SBA-15 and α-Ag_2WO_4, which corroborate the obtaining of supported nanomaterial.

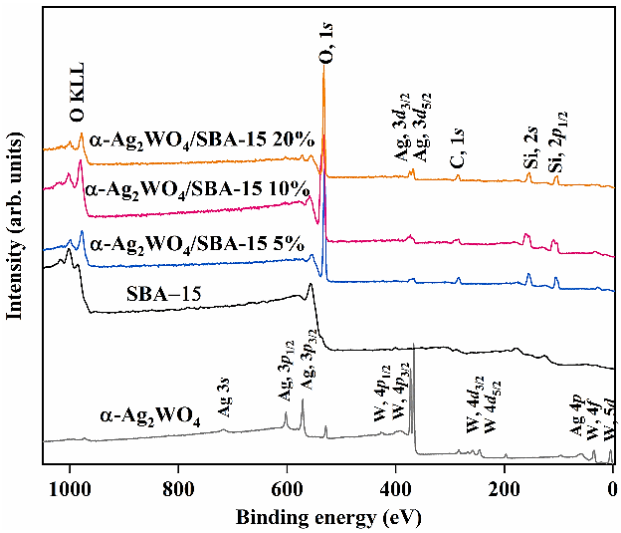

Fig. 3. XPS spectra of adsorbents

XPS spectra at high resolution of O 1s can show interactions between the α-Ag_2WO_4 and SBA-15. In previous work by our research group (Silva et al., 2020b), the spectra at high resolution of O 1s to α-Ag_2WO_4 and SBA-15 were reported. The deconvoluted spectrum of O1s of α-Ag_2WO_4 shows three components with binding energy 530.2; 530.7 and 532 eV related, respectively, to Ag–O, W–O, and O–H bonds (Bernard Ng and Fan, 2016; Silva et al., 2020b; Zhu et al., 2017). The deconvoluted spectrum of O 1s to SBA-15 shows two components of binding energy 533.3 and 534.6 eV (Silva et al., 2020b), which are related to the OH of water molecules chemisorbed on the surface of SBA-15 and Si–O–Si bonds (Qiang et al., 2019; Silva et al., 2020b; Zhu et al., 2017). Fig. 4(a-c) presents peaks of α-Ag_2WO_4/SBA-15 x% (x = 5, 10, and 20) with binding energies between 533 and 540 eV, which are associated to the interactions of molecule surface water with the crystal surface and the bonds O–Ag–O, Si–O–Si, and O–W–O. These energies of bonds are higher than those reported in the literature to α-Ag_2WO_4 and SBA-15 (Bernard Ng and Fan, 2016; Qiang et al., 2019; Silva et al., 2020b; Wisniewska et al., 2019; Zhu et al., 2017). This should be related to neighborhood effect due to chemical interactions (Ag, W, O and Si atoms). Therefore, XPS analysis corroborated the coexistence of α-Ag_2WO_4 and SBA-15 support in the nanocomposites (α-Ag_2WO_4/SBA-15 x%), as indicate by deviations of energy values associated to the different environment chemical generated by Ag, O, W, and Si atoms.

Table 1. Textural property and zeta potential of adsorbents

Adsorbents	S_{BET} ($m^2\ g^{-1}$)	$S_{external}$ ($m^2\ g^{-1}$)	S_{micro} ($m^2\ g^{-1}$)	V_{poro} ($cm^3\ g^{-1}$)	V_{micro} ($cm^3\ g^{-1}$)	*Dp* (nm)	*ζ* (mV, pH 6)
SBA-15*	677.0	572.7	104.3	0.86	0.04	6.4	-63.3
α-Ag_2WO_4*	21.0	22.9	15.4	0.12	-	31.81	-66.9
α-Ag_2WO_4/SBA-15 5%	532.5	463.7	68.8	0.80	0.04	6.7	-76.9
α-Ag_2WO_4/SBA-15 10%	577.7	485.7	91.9	0.81	0.04	6.6	-67.6
α-Ag_2WO_4/SBA-15 20%	521.9	455.8	66.2	0.75	0.02	6.7	-60.4

** Reprinted with permission from **Springer Nature Customer Service Centre GmbH** (Silva et al., 2020b). COPYRIGHT 2020 Springer Nature*

3.5. RhB adsorption study

Figure 5a shows that adsorption capacity of α-Ag_2WO_4/SBA-15 20% and α-Ag_2WO_4 are similar and far superior to that of adsorbents SBA-15, α-Ag_2WO_4/SBA-15 10%, and α-Ag_2WO_4/SBA-15 5%. The adsorption equilibrium time was 5 minutes for α-Ag_2WO_4 and 20 minutes for SBA-15, α-Ag_2WO_4/SBA-15 5%, α-Ag_2WO_4/SBA-15 10%, and α-Ag_2WO_4/SBA-15 20%. This equilibrium time is consistent with other studies of Rhodamine B adsorption reported in literature (Cheng et al., 2017; Cheng et al., 2018; Dutta et al., 2014). The good performance of α-Ag_2WO_4 and α-Ag_2WO_4/SBA-15 20% indicates that the mass of α-Ag_2WO_4 is important in removal of RhB from aqueous solutions.

Figure 5b shows the influence of pH in adsorption of RhB. Adsorption is high, at pH < 3.7 (value of RhB pKa), because the predominate cationic form of RhB is easily attracted by negative charge of the adsorbents. The literature reports high adsorption of RhB at pH 3-4 (Hayeeye et al., 2017; Inyinbor et al., 2015; Silva et al., 2020a). Adsorption of RhB decreases at pH > 3.7, due to repulsion between the negative charges of the adsorbent and the dye. The study of pH indicated that electrostatic interaction is the determining factor in adsorption.

Table 2 shows that the adsorbents are selective because they all have high adsorption capacity at low concentrations of RhB dye (2.5 mg L^{-1}). α-Ag_2WO_4 and α-Ag_2WO_4/SBA-15 20% have adsorption capacity related to concentration of RhB dye solution (2.5, 5, and 10 mg L^{-1}). The adsorbents of α-Ag_2WO_4/SBA-15 x% (x = 5 and 10) and SBA-15 are not following this tendency, which could be related at lower adsorption capacity of SBA-15. The lower performance of SBA-15 for adsorption of RhB can be understood by the mechanism and thermodynamic parameters of adsorption (Silva et al., 2020b). The SBA-15 owing her groups silanols interact with water molecules creating positive charge, which can to repel of positive groups of RhB ($-N^+$) yielding little adsorption of RhB (Silva et al., 2020b)

The adsorption capacity of α-Ag_2WO_4/SBA-15 20% is no similar to α-Ag_2WO_4 at concentrations of RhB 15 and 20 mg L^{-1}. This suggests that the concentrations of 15 and 20 mg L^{-1} saturate the active sites of α-Ag_2WO_4/SBA-15 20%, which has lower adsorption capacity of RhB at the aforementioned concentrations. α-Ag_2WO_4/SBA-15 20% presents removal efficiency close to 98% similar to α-Ag_2WO_4 at 10 mg L^{-1} RhB concentration.

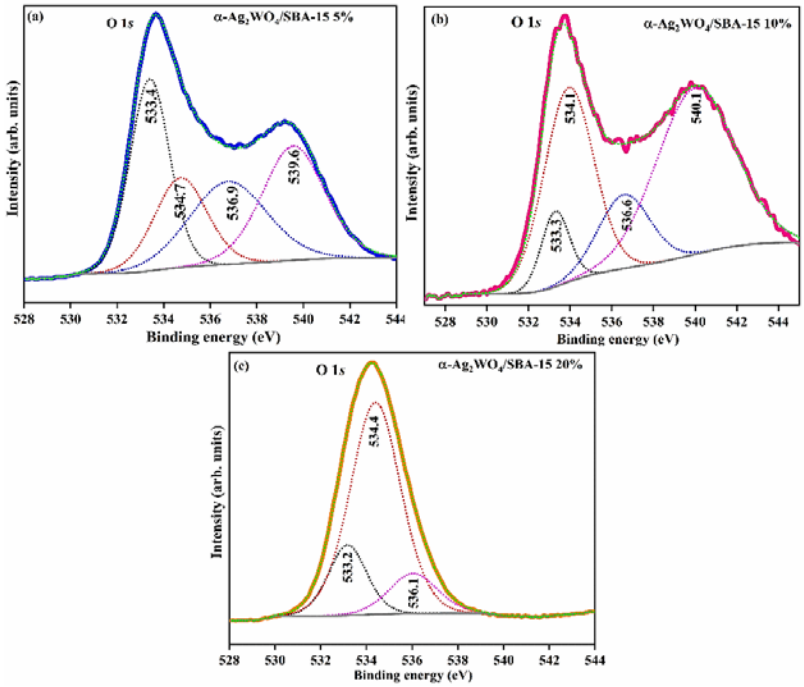

Fig. 4. High-resolution spectra for O 1s of adsorbents: (a) α-Ag_2WO_4/SBA-15 5%; (b) α-Ag_2WO_4/SBA-15 10%, and (c) α-Ag_2WO_4/SBA-15 20%

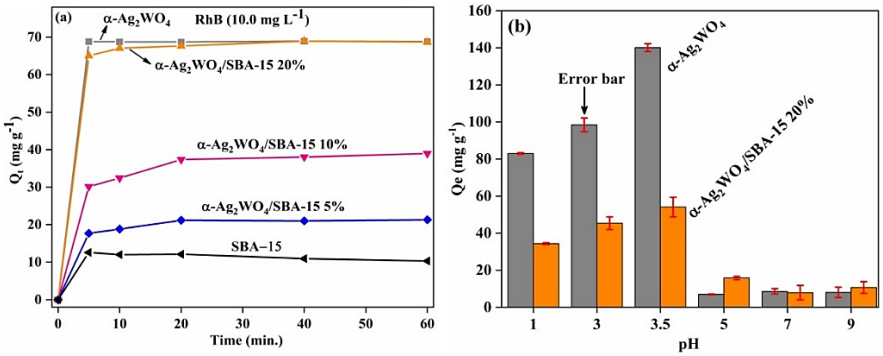

Fig. 5. Effect of contact time (a) and pH (b) on the adsorption of RhB onto adsorbents

Table 2. Adsorption capacity and adsorbents efficiency for the RhB dye

Qe(mg g^{-1})					
Adsorbents	***Concentrations (mg L^{-1})***				
	2.5	***5***	***10***	***15***	***20***
SBA-15*****	11.2	17.5	10.3	24.6	20.9
α-Ag$_2$WO$_4$*****	16.4	34.2	68.8	105.5	121.2
α-Ag$_2$WO$_4$/SBA-15 5%	11.2	18.0	21.3	27.8	23.3
α-Ag$_2$WO$_4$/SBA-15 10%	16.1	31.6	38.9	37.8	41.3
α-Ag$_2$WO$_4$/SBA-15 20%	16.9	32.7	68.7	90.1	92.3
Adsorbents efficiency					
SBA-15*****	62.8%	49.0%	14.4%	22.9%	14.6%
α-Ag$_2$WO$_4$*****	91.8%	95.7%	98.0%	98.2%	99.1%
α-Ag$_2$WO$_4$/SBA-15 5%	62.6%	50.5%	29.8%	26.0%	16.3%
α-Ag$_2$WO$_4$/SBA-15 10%	90.4%	88.6%	54.6%	35.3%	28.9%
α-Ag$_2$WO$_4$/SBA-15 20%	94.7%	91.7%	97.3%	84.9%	64.6%

** Reprinted with permission from **Springer Nature Customer Service Centre GmbH** (Silva et al., 2020b). COPYRIGHT 2020 Springer Nature*

The better adsorptive performance of α-Ag$_2$WO$_4$ and α-Ag$_2$WO$_4$/SBA-15 may be associated to negative charges of α-Ag$_2$WO$_4$ due to the O atoms attracting the -N$^+$ groups of RhB dye (Silva et al., 2020b). The performance of α-Ag$_2$WO$_4$/SBA-15 is associated to α-Ag$_2$WO$_4$ amount and follows the order: α-Ag$_2$WO$_4$/SBA-15 5% <Ag$_2$WO$_4$/SBA-15 10% <Ag$_2$WO$_4$/SBA-15 20%. This suggests that the negative charges of α-Ag$_2$WO$_4$ are proportional to its mass, which needs to be sufficient to overcome the repulsions between the positive groups of SBA-15 and RhB dye. α-Ag$_2$WO$_4$ supported on SBA-15 improves its adsorption capacity, as can be seen in the similar performance of α-Ag$_2$WO$_4$ and Ag$_2$WO$_4$/SBA-15 20%, even the last one having only 20 wt.% of Ag$_2$WO$_4$. This fact may be related to a better distribution of activity sites on supported material than on pure α-Ag$_2$WO$_4$, which can make it more available to RhB molecules during the adsorption process.

3.6. Kinetics study

The kinetics of RhB adsorption fit pseudo-second order model as can be seen in table 3. The linear regression coefficients (R^2) are close to one, and the adsorption capacity (q_e mg g^{-1}) determined by experimental tests and parameter graphic agree. Therefore, the kinetics of RhB adsorption onto adsorbents follows pseudo-second order (Cheng et al., 2017; do Nascimento et al., 2014; Silva et al., 2020b; Wang et al., 2014). Pseudo-second order model suggests that the mechanism influences the adsorption capacity of adsorbents. The pseudo-first order model is not fit for kinetics of RhB adsorption as shown by R^2 (correlation coefficients) and discrepancy of adsorption capacity experimental ($q_{e\ exp.}$) and calculated (($q_{e\ calc.}$) (Cheng et al., 2017; do Nascimento et al., 2014).

3.7. Adsorption isotherms

Table 4 shows that the data adsorption of RhB onto adsorbents fits Langmuir model (Chang et al., 2020; Cheng et al., 2018). For all adsorbents, q_e (mg g^{-1}) calculated by the Langmuir model and the experimental data are similar, and linear regression coefficients (R^2) are close to 1. The Langmuir model indicates monolayer adsorption at particular adsorbent sites without interaction between substrate molecules (Chang et al., 2020; Cheng et al., 2017; Cheng et al., 2018). α-Ag$_2$WO$_4$/SBA-15 20% and α-Ag$_2$WO$_4$ exhibit maximum adsorption capacity, extracted from Langmuir isotherm, equal 55 mg g^{-1} and 145 mg g^{-1}, respectively. Although α-Ag$_2$WO$_4$/SBA-15 20% has only 20% of α-Ag$_2$WO$_4$, it has about 38% of performance of α-Ag$_2$WO$_4$ pure. This indicates that the support can improve the performance of α-Ag$_2$WO$_4$ as adsorbent. The values of dimensionless separation factors ($0 < R_L < 1$) reveal favorable RhB adsorption. The experimental data of RhB adsorption in adsorbents do not adjust to Freundlich and Temkin models (Table 4) because values of R^2 are far from the

unit (Cheng et al., 2018; do Nascimento et al., 2014; Zhang et al., 2018).

3.8. Effect of temperature

Influence of temperature, dosage, and KCl in adsorption capacity of adsorbents for RhB, as well as the desorption of RhB are illustrate in Fig. 6. Figure 6a illustrates that increased temperature favors the adsorption onto α-Ag_2WO_4/SBA-15 20% and α-Ag_2WO_4. Temperature increase may facilitate ion mobility or activate sites (Hayeeye et al., 2017; Sousa et al., 2018). In SBA-15, the increase of temperature reduces the adsorption capacity, which indicates that the process of RhB adsorption on SBA-15 is exothermic.

Thermodynamic parameters at temperatures of 298, 308, and 318 K are in Table 5. As seen in Table 5, α-Ag_2WO_4/SBA-15 20% and α-Ag_2WO_4 adsorbents have positive ΔH and ΔS, indicating a reversible endothermic process (Shen and Gondal, 2017; Silva et al., 2020b). SBA-15 has negative ΔH and ΔS, showing that it is exothermic to this adsorbent, which means reduction in the randomness at liquid-solid interface of the adsorption (Inyinbor et al., 2015; Silva et al., 2020b). The ΔG reduces with increasing temperature for α-Ag_2WO_4/SBA-15 20% and α-Ag_2WO_4, which must be associated to the raise of species mobility in aqueous solution and/or activation of sites (Hayeeye et al., 2017; Sousa et al., 2018). The temperature raises promoted increase ΔG for SBA-15, which indicates adsorption is less favorable or spontaneous in this adsorbent.

The values of thermodynamic parameters (ΔG, ΔH, and ΔS) of SBA-15 are coherent with its lower adsorption of RhB dye. However, the SBA-15 support facilitates separation between adsorbent and dye and improves the adsorption capacity owing to the high specific area, which can disperse α-Ag_2WO_4 nanocrystals.

3.9. Effect of adsorbent dosage

Fig 6b shows that the dosage of α-Ag_2WO_4 (0.352 g L^{-1}) achieves 100% removal efficiency of RhB 50 ppm, and the dosage of 1.050 g L^{-1} of α-Ag_2WO_4/SBA-15 20% exhibits similar results. Dosage of α-Ag_2WO_4/SBA-15 20% (1.050 g L^{-1}) is three times the dosage of α-Ag_2WO_4 (0.352 g L^{-1}); but the dosage expected, according with percentage (mass ratio) of silver tungstate, would be five times. This reinforces that the support SBA-15 improved the performance of α-Ag_2WO_4 /SBA-15 20% for adsorption of RhB.

Table 3. Parameter of adsorption kinetics of RhB onto adsorbents

Adsorbents	***Pseudo-first order kinetics***			
	$Q_{e\ calc}$ (mg g^{-1})	$Q_{e\ exp.}$ (mg g^{-1})	K_1 (min^{-1})	R^2
SBA-15*****	99.46	19.35	0.13	0.47
α-Ag_2WO_4*****	432.29	141.60	0.78	0.85
α-Ag_2WO_4/SBA-15 5%	197.09	23.78	0.14	0.94
α-Ag_2WO_4/SBA-15 10%	216.64	35.57	0.068	0.98
α-Ag_2WO_4/SBA-15 20%	224.73	52.35	0.066	0.89
	Pseudo-second order kinetics			
	$Q_{e\ calc}$ (mg g^{-1})	$Q_{e\ exp.}$ (mg g^{-1})	K_2 (g mg^{-1} min^{-1})	R^2
SBA-15*****	19.61	19.35	0.053	0.99
α-Ag_2WO_4*****	144.92	141.60	0.25	0.99
α-Ag_2WO_4/SBA-15 5%	25.05	23.78	0.012	0.99
α-Ag_2WO_4/SBA-15 10%	36.27	35.57	0.014	0.99
α-Ag_2WO_4/SBA-15 20%	54.41	52.36	0.0083	0.98

** Reprinted with permission from **Springer Nature Customer Service Centre GmbH** (Silva et al., 2020b). COPYRIGHT 2020 Springer Nature*

Table 4. Parameters of Langmuir, Freundlich, and Temkin isotherm models

Adsorbents	***Langmuir***			
	$Q_{máx}$ (mg g^{-1})	K_L (L mg^{-1})	R^2	R_L
SBA-15*****	21.71	0.75	0.98	0.072
α-Ag_2WO_4*****	144.93	1.82	0.99	0.0055
α-Ag_2WO_4/SBA-15 5%	19.04	0.67	0.99	0.069
α-Ag_2WO_4/SBA-15 10%	24.81	4.03	0.99	0.0010
α-Ag_2WO_4/SBA-15 20%	54.94	4.67	0.99	0.010

	Freundlich			***Temkin***		
	n	K_f (L g^{-1})	R^2	n_T	K_T (L g^{-1})	R^2
SBA-15*****	0.37	3.2 x 10^{-3}	0.90	0.22	1.3 x10^3	0.88
α-Ag_2WO_4*****	3.90	64.74	0.38	0.059	2.3 x 10^{-2}	0.37
α-Ag_2WO_4/SBA-15 5%	7.82	18.77	0.49	0.33	20.18	0.91
α-Ag_2WO_4/SBA-15 10%	3.91	34.38	0.54	0.43	5.7 x 10^3	0.51
α-Ag_2WO_4/SBA-15 20%	3.35	67.58	0.57	0.12	156.02	0.54

****** Reprinted with permission from **Springer Nature Customer Service Centre GmbH** (Silva et al., 2020b). COPYRIGHT 2020 Springer Nature*

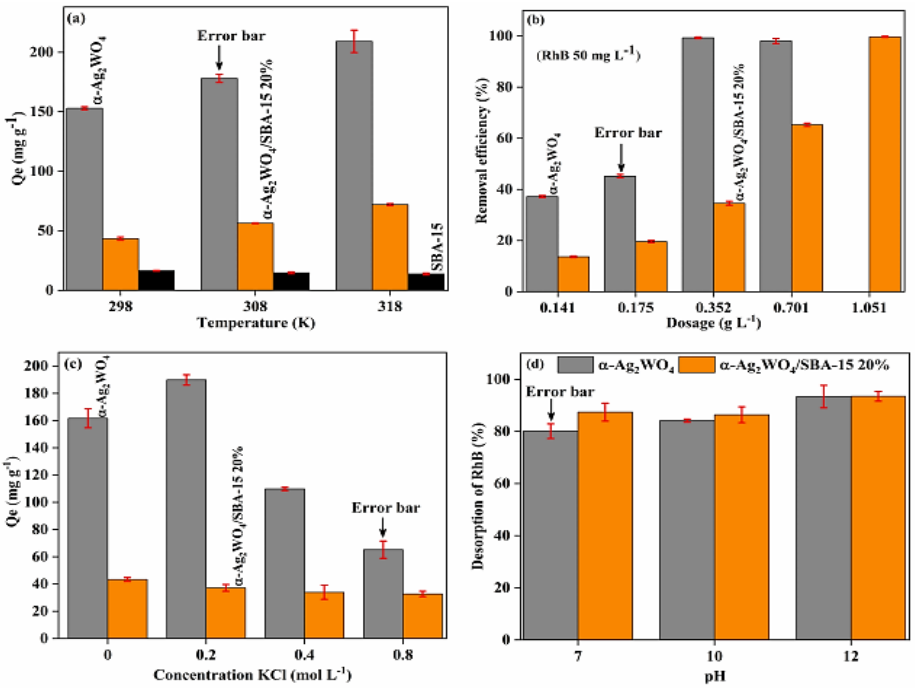

Fig. 6. Influence of (a) temperature, (b) dosage, (c) KCl in adsorption capacity of adsorbents for RhB, and (d) Desorption of RhB from adsorbents

Table 5. Thermodynamic parameters for adsorption of RhB onto α-Ag$_2$WO$_4$, SBA-15, and α-Ag$_2$WO$_4$/SBA-15 20%

Adsorbents	***Thermodynamics parameters***				
	ΔH (KJ/ mol)	***ΔS (J/ mol K)***	***ΔG (KJ / mol)***		
			298 K	***308 K***	***318 K***
SBA-15*	-8.7	-23.0	-1.9	-1.6	-1.4
α-Ag$_2$WO$_4$*	34.3	132.2	-5.2	-6.3	-7.8
α-Ag$_2$WO$_4$/SBA-15 20%	34.7	125.4	-2.8	-3.8	-5.3

***** *Reprinted with permission from* ***Springer Nature Customer Service Centre GmbH*** *(Silva et al., 2020b). COPYRIGHT 2020 Springer Nature*

3.10. Role of KCl

The effect of KCl was studied in order to observe the influence of ions on the contaminant adsorption (RhB) process. In addition, this study clarifies the electrostatic nature of the interactions between adsorbent and contaminant. Effect of KCl on the removal of RhB by α-Ag$_2$WO$_4$ and α-Ag$_2$WO$_4$/SBA-15 20% is shown in Fig. 6c. α-Ag$_2$WO$_4$ exhibited slightly increased adsorption capacity in concentration of KCl 0.2 mol L^{-1}. At this concentration, RhB may be less soluble, facilitating diffusion or mass transfer to adsorbents (Peng et al., 2016). For α-Ag$_2$WO$_4$, adsorption capacity reduced in concentrations of KCl greater than 0.2 mol L^{-1}, this indicates a competition between ion K$^+$ and dye (RhB) for adsorption sites (Silva et al., 2020a). α-Ag$_2$WO$_4$SBA-15 20% has adsorption capacity smoothly affected, which suggest dispersion α-Ag$_2$WO$_4$ nanocrystals in the surface of SBA-15 minimizing the aforementioned competition between ions and adsorbate.

3.11. Desorption of RhB from α-Ag$_2$WO$_4$/SBA-15 20% and α-Ag$_2$WO$_4$

The removal of RhB from adsorbents (α-Ag$_2$WO$_4$/SBA-15 20% and α-Ag$_2$WO$_4$) was efficient and quick, employing changes of pH. Fig. 6d shows that 80% and 87% of RhB were recuperated from the adsorbents α-Ag$_2$WO$_4$ and α-Ag$_2$WO$_4$/SBA-15 20%, respectively, at pH 7. The recuperation attains 93% for both adsorbents at pH 12. The easy desorption of RhB evidences that the adsorption is driven mainly by electrostatic forces.

4. Conclusions

α-Ag$_2$WO$_4$ nanocrystals and α-Ag$_2$WO$_4$/SBA-15 x% (x = 5, 10, and 20) were obtained by sonochemical and post-synthesis methods, respectively. α-Ag$_2$WO$_4$/SBA-15 x% maintained structures of both materials (α-Ag$_2$WO$_4$ and SBA-15) and exhibited textural properties analogous to SBA-15. The experimental data from adsorption of RhB onto α-Ag$_2$WO$_4$, SBA-15 and α-Ag$_2$WO$_4$ x% (x = 5, 10 and 20) were well fitted to Langmuir model and pseudo-second order kinetics. The performance of α-Ag$_2$WO$_4$/SBA-15 x% in RhB adsorption was dependent on the percentage (mass ratio) of α-Ag$_2$WO$_4$, with the best performance achieved by α-Ag$_2$WO$_4$/SBA-15 20%. The performance of α-Ag$_2$WO$_4$/SBA-15 20% and α-Ag$_2$WO$_4$ for RhB adsorption was uniformly affected by KCl, but highly pH-dependent (pH ~ 3.5 was the best).

The process of RhB adsorption was endothermic, spontaneous, and compatible with physisorption. For SBA-15, RhB adsorption was exothermic and less favorable, which clarified its lower performance. The main step in the mechanism of the RhB adsorption onto adsorbents must be electrostatic interactions between the positive and negative charges of the dye and the adsorbents, respectively. This study indicated that α-Ag_2WO_4/SBA-15 x% has improved performance for adsorption of cationic dyes due to surface area of support and percentage of α-Ag_2WO_4.

References

Andrade Neto N.F., Oliveira P.M., Bomio M.R.D., Motta F.V., (2019), Effect of temperature on the morphology and optical properties of Ag_2WO_4 obtained by the co-precipitation method: Photocatalytic activity, *Ceramics International*, **45**, 15205-15212.

Araújo M.M., Silva L.K.R., Sczancoski J.C., Orlandi M.O., Longo E., Santos A.G.D., Santos R.S., Luz Jr. G.E., Cavalcante L.S., (2016), Anatase TiO_2 nanocrystals anchored at inside of SBA-15 mesopores and their optical behavior, *Applied Surface Science*, **389**, 1137-1147.

Bernard Ng C.H., Fan W.Y., (2016), Preparation of highly uniform 1-dimensional α-Ag_2WO_4 nanostructures with controllable aspect ratio and study of the growth mechanism, *CrystEngComm*, **18**, 8010-8019.

Chai Y., Wang L., Ren J., Dai W.L., (2015), A novel visible light-driven Ag_3PO_4/SBA-15 nanocomposite Preparation and application in the photo-degradation of pollutants, *Applied Surface Science*, **324**, 212-220.

Chang S., Zhang Q., Lu Y., Wu S., Wang W., (2020), High-efficiency and selective adsorption of organic pollutants by magnetic $CoFe_2O_4$/grapheme oxide adsorbents: Experimental and molecular dynamics simulation study, *Separation and Purification Technology*, **238**, 116400.

Chaouki Z., Zaitan H., Bawdali M., Vasarevičius S., Mažeikienė A., (2020), Oil removal from refinery wastewater through adsorption on low cost natural biosorbents, *Environmental Engineering and Management Journal*, **19**, 105-112.

Chen H., Xu Y., (2014), Photoactivity and stability of Ag_2WO_4 for organic degradation in aqueous suspensions, *Applied Surface Science*, **319**, 319-323.

Cheng Z.L., Li Y.X., Liu Z., (2017), Novel adsorption materials based on graphene oxide/Beta zeolite composite materials and their adsorption performance for Rhodamine B, *Journal of Alloy and Compounds*, **708**, 255-263.

Cheng Z.L., Li Y.X., Liu Z., (2018), Study on adsorption of Rhodamine B onto Beta zeolites by tuning SiO_2/Al_2O_3 ratio, *Ecotoxicology and Environmental Safety*, **148**, 585-592.

Costa T.M.S., Lima M.S., Cruz Filho J.F., Silva L.F., Santos R.S., Luz Jr.G.E., (2018), Synthesis, characterization, and photocatalytic activity of Ag_3PO_4 /SBA-15 in ciprofloxacin degradation under polychromatic irradiation, *Journal of Photochemistry and Photobiology A: Chemistry*, **364**, 461-471.

do Nascimento R.F., de Lima A.C.A., Vidal C.B., Melo D.Q., Raulino G.S., (2014), Equilíbrio de Adsorção, Adsorção: aspectos teóricos e aplicações ambientais, Imprensa Universitária (Ed.), edições UFC, Fortaleza, 23-48.

Dutta A.K., Ghorai U.K., Chattopadhyay K.K., Banerjee D., (2018), Removal of textile dyes by carbon nanotubes: A comparison between adsorption and UV assisted photocatalysis, *Physica E: Low-dimensional Systems and Nanostructures*, **99**, 6-15.

Dutta D.P., Singh A., Ballal A., Tyagi A.K., (2014), High Adsorption capacity for cationic dye removal and antibacterial properties of sonochemically synthesized Ag_2WO_4 nanorods, *European Journal of Inorganic Chemistry*, **33**, 5724-5732.

Errais E., Duplay J., Darragi F., (2010), Textile dye removal by natural clay – case study of Fouchana Tunisian clay, *Environmental Technology*, **31**, 373-380.

Foggi C.C., Fabbro M.T., Santos L.P.S., de Santana Y.V.B., Vergani C.E., Machado A.L., Cordoncillo E., Andrés J., Longo E., (2017), Synthesis and evaluation of α-Ag_2WO_4 as novel antifungal agent, *Chemical Physics Letters*, **674**, 125-129.

Freundlich H., (1926), *Colloid and Capillary Chemistry*, Methuen & Co. Ltd., London, UK.

Hamza W., Dammak N., Hadjltaiet H.B., Eloussaief M., Benzina M., (2018), Sono-assisted adsorption of Cristal Violet dye onto Tunisian Smectite Clay: Characterization, kinetics and adsorption isotherms, *Ecotoxicology and Environmental Safety*, **163**, 365-371.

Hayeeye F., Sattara M., Chinpab W., Sirichotea O., (2017), Kinetics and thermodynamics of Rhodamine B adsorption by gelatin/activated carbon composite beads, *Colloids and Surfaces A: Physicochemical and Engineering Aspects*, **513**, 259-266.

He H., Xue S., Wu Z., Yu C., Yang K., Peng G., Zhou W., Li D., (2016), Sonochemical fabrication, characterization and enhanced photocatalytic performance of Ag_2S/Ag_2WO_4 composite microrods, *Chinese Journal of Catalysis*, **37**, 1841-1850.

Ho Y.S., Mckay G.K., (1998), Kinetic models for the sorption of dye from aqueous solution by wood, *Transactions of the Institution of Chemical Engineering*, **76B**, 183-191.

Inyinbor A.A., Adekola F.A., Olatunji G.A., (2015), Adsorption of Rhodamine B dye from aqueous solution on Irvingia gabonensis biomass: Kinetics and thermodynamics studies, *South African Journal of Chemistry*, **68**, 115-125.

Jin M., Guo Z., Lv Z., (2019), Immobilization of tungsten chelate complexes on functionalized mesoporous silica SBA-15 as heterogeneous catalysts for oxidation of cyclopentene, *Journal of Materials Science*, **54**, 6853-6866.

Langmuir I., (1916), The dissociation of hydrogen into atoms III. The mechanism of the reaction, *Journal of the American Chemical Society*, **38**, 1145-1156.

Li B., Mu B., Yang Y., (2019), Feasibility of industrial-scale treatment of dye wastewater via bio-adsorption technology, *Bioresource Technology*, **277**, 157-170.

Li Y., Jin R., Fang X., Yang Y., Yang M., Liu X., Xing Y., Song S., (2016), In situ loading of Ag_2WO_4 on ultrathin g-C_3N_4 nanosheets with highly enhanced photocatalytic performance, *Journal of Hazardous Materials*, **313**, 219-228.

Li Y., Li Y., Ma S., Wang P., Hou Q., Han J., Zhan S., (2017), Efficient water disinfection with Ag_2WO_4-doped mesoporous g-C_3N_4 under visible light, *Journal of Hazardous Materials*, **338**, 33-46.

Longo V.M., de Foggi C.C., Ferrer M.M., Gouveia A.F., André R.S., Avansi W., Vergani C.E., Machado A.L., Andrés J., Cavalcante L.S., Hernandes A.C., Longo E., (2014), Potentiated electron transference in α- Ag_2WO_4

microcrystals with Ag nanofilaments as microbial agent, *The Journal of Physical Chemistry A*, **118**, 5769-5778.

Macedo N.G., Gouveia A.F., Roca R.A., Assis M., Gracia L., Andrés J., Leite E.R., Longo E., (2018), Surfactant-mediated morphology and photocatalytic activity of α-Ag_2WO_4 material, *The Journal of Physical Chemistry C*, **122**, 8667-8679.

Peng X., Hu F., Dai H., Xiong Q., Xu C., (2016), Study of the adsorption mechanisms of ciprofloxacin antibiotics onto graphitic ordered mesoporous carbons, *Journal of Taiwan Institute Chemical Engineers*, **65**, 472-481.

Periyaraman P., M., Karan S., Ponnusamy S., K., Vaidyanathan V., Vasanthakumar S., Dhanasekaran A., Subramanian S., (2019), Adsorption of an anionic dye onto native and chemically modified agricultural waste, *Environmental Engineering and Management Journal*, **18,** 257-270.

Qiang T., Song Y., Zhao J., Li J., (2019), Controlled incorporation homogeneous Ti-doped SBA-15 for improving methylene blue adsorption capacity, *Journal of Alloys and Compounds*, **770**, 792-802.

Qin Q., Ma J., Liu K., (2009), Adsorption of anionic dyes on ammonium-functionalized MCM-41, *Journal of Hazardous Materials*, **162**, 133-139.

Rachna K., Agarwal A., Singh N.B., (2018), Preparation and characterization of zinc ferrite-Polyaniline nanocomposite for removal of Rhodamine B dye from aqueous solution, *Environmental Nanotechnology, Monitoring and Management*, **9**, 154-163.

Roca R.A., Sczancoski J.C., Nogueira I.C., Fabbro M.T., Alves H.C., Gracia L., Santos L.P.S., de Sousa C.P., Andrés J., Luz Jr G.E., Longo E., Cavalcante L.S., (2015), Facet-dependent photocatalytic and antibacterial properties of α-Ag_2WO_4 crystals: combining experimental data and theoretical insights, *Catalysis Science and Technology*, **5**, 4091-4107.

Senthil R.A., Osman S., Pan J., Khan A., Yang V., Kumar T.R., Sun Y., Lin Y., Liu X., Manikandan A., (2020), One-pot preparation of AgBr/α-Ag_2WO_4 composite with superior photocatalytic activity under visible-light irradiation, *Colloids and Surfaces A*, **586**, 124079.

Shen K., Gondal M.A., (2017), Removal of hazardous Rhodamine dye from water by adsorption onto exhausted coffee ground, *Journal of Saudi Chemical Society*, **21**, 120-127.

Silva F.C.M., Silva L.K.R., Santos A.G.D., Caldeira V.P.S., Cruz-Filho J.F., Cavalcante L.S., Longo E., Luz Jr G.E., (2020b), Structural refinement, morphological features, optical properties, and adsorption capacity of α-Ag_2WO_4 nanocrystals/SBA-15 mesoporous on Rhodamine B dye, *Journal Inorganic Organometallic Polymers*, **30**, 3626-3645.

Silva F.C.M., Costa M.J., Silva L.K.R., Batista A.M., Luz Jr. G.E., (2019), Functionalization methods of SBA-15 mesoporous molecular sieve: a brief overview, *SN Applied Sciences*, **1**, doi.org/10.1007/s42452-019-0677-z.

Silva M.S., Silva L.S., Ferreira F.J.L., Bezerra R.D.S., Marques T.M.F., Meneguin A.B., Barud H.S., Osajima J.A., Silva Filho E.C., (2020a), Study of interactions between organic contaminants and a new phosphated biopolymer derived from cellulose, *International Journal of Biological Macromolecules*, **146**, 668-677.

Singh S., Kumar R., Setiabudi H.D., Nanda S., Vo D.V.N., (2018), Advanced synthesis strategies of mesoporous SBA-15 supported catalysts for catalytic reforming applications: A state-of-the-art review, *Applied Catalysis A: General*, **559**, 57-74.

Skarstad P.M., Geller S., (1975), $(W_4O_{16})^{8-}$ Polyion in the high temperature modification of silver tungstate, *Materials Research Bulletin*, **10**, 791-799.

Sousa W.R.D.N., Oliveira A.R., Cruz Filho J.F., Dantas T.C.M., Santos A.G.D., Caldeira V.P.S., Luz Jr. G.E., (2018), Ciprofloxacin Adsorption on ZnO Supported on SBA-15, *Water, Air, and Soil Pollution*, **229**, 125-131.

Szewczyk A., Prokopowicz M., Sawicki W., Majda D., Walker G., (2019), Aminopropyl-functionalized mesoporous silica SBA-15 as drug carrier for cefazolin: adsorption profiles, release studies, and mineralization potential, *Microporous and Mesoporous Materials*, **274**, 113-126.

Wang P., Cheng M., Zhang Z., (2014), On different photodecomposition behaviors of Rhodamine B on laponite and montmorillonite clay under visible light irradiation, *Journal of Saudi Chemical Society*, **18**, 308-316.

Wisniewska J., Grzelak K., Huang S.P., Sobczak I., Yang C.M., Ziolek M., (2019), The influence of Zr presence in short channel SBA-15 on state and activity of metallic modifiers (Ag, Au, Cu, Fe), *Catalysis Today*, On line at: https://doi.org/10.1016/j.cattod.2019.05.012.

Xu D., Cheng B., Cao S., Yu J., (2015), Enhanced photocatalytic activity and stability of Z-scheme Ag_2CrO_4-GO composite photocatalysts for organic pollutant degradation, *Applied Catalysis B: Environmental*, **164**, 380-388.

Xu H., Cao Y., Xie J., Hu J., Li Y., Jia D., (2018), A construction of Ag-modified raspberry-like AgCl/Ag_2WO_4 with excellent visible-light photocatalytic property and stability, *Materials Research Bulletin*, **102**, 342-352.

Zhang H., Niu J., Yin X., Guo Y., Cheng F., (2020), Role of inherent pyrite in coal on physicochemical structure of activated carbon and adsorption capacity, *Fuel*, **262**, 116527.

Zhang J., Yan X., Hu X., Feng R., Zhou M., (2018), Direct carbonization of Zn/Co zeolitic imidazolate frameworks for efficient adsorption of Rhodamine B, *Chemical Engineering Journal*, **347**, 640-647.

Zhao D., Feng J., Huo Q., Melosh N., Fredrickson G.H., Chmelka B.F., Stucky G.D., (1998a), Triblock copolymer synthesis of mesoporous silica with periodic 50 to 300 Angstrom pores, *Science*, **279**, 548-552.

Zhao D., Huo Q., Feng J., Chmelka B.F., Stucky G.D., (1998b), Nonionic triblock and star diblock copolymer and oligomeric surfactant syntheses of highly ordered, hydrothermally stable, mesoporous silica structures, *Journal of American Chemical Society*, **120**, 6024-6036.

Zhou Y., Lu J., Zhou Y., Liu Y., (2019), Recent advances for dyes removal using novel adsorbents: A review, *Environmental Pollution*, **252**, 352-365.

Zhu B., Xia P., Li Y., Ho W., Yu J., (2017), Fabrication and photocatalytic activity enhanced mechanism of direct Z-scheme g-C_3N_4/Ag_2WO_4 photocatalyst, *Applied Surface Science*, **391**, 175-183.